Low-Observable Nonlinear Trajectory Generation for Unmanned Air Vehicles *

K. Misovec †, T. Inanc ‡, J. Wohletz §, R. M. Murray ¶

Submitted to the IEEE Conference on Decision and Control 2003

Keywords: Trajectory Generation, Path Planning, Low-Observable, UAV, RADAR, Probability of Detection

Abstract

This paper explores low observability flight path planning of unmanned air vehicles (UAV's) in the presence of radar detection systems. The probability of detection model of an aircraft near an enemy radar depends on aircraft attitude, range, and configuration. A detection model is coupled with a simplified aircraft dynamics model. The Nonlinear Trajectory Generation (NTG) software package developed at Caltech is used. The NTG algorithm is a gradient descent optimization method that combines three technologies: B–splines, output space collocation and nonlinear optimization tools. Implementations are formulated with temporal constraints that allow periods of high observability interspersed with periods of low observability. Illustrative examples of optimized routes for low observability are presented.

1 Introduction

As the development of new unmanned vehicles progresses, research focused on coordinating large teams of these vehicles has highlighted many new challenges for control. Due to complexity of large–scale unmanned vehicle systems, several control design algorithms in a hierarchical, distributed manner have been proposed. The Mixed Initiative Control of Automa–teams (MICA) of DARPA studies a multi–layer planning, assessment, and control architecture of distributed semi–autonomous forces with collective obectives. The approach taken in the DARPA MICA program is to decompose the control design into several layers: TCT–Team Composition and Tasking– for specifying group level tasks, TDT–Team Dynamics and Tactics– for tasking team activities, CPP–Cooperative Path Planning– for generating feasible missions. At the CPP level of the MICA, the design goals are to command the vehicles to pursue dynamically feasible routes, such as those with speed and turning rate limits, while avoiding threats and collisions with other vehicles. Driven by battlespace management needs, real-world threats can be much more complex than those modeled in prior trajectory generation work. The detectability of an aircraft traveling near an enemy radar depends on more than just the distance to the radar; it depends on the aircraft attitude and configuration as well. This feature in the threat model introduces nonconvexities, path dependencies, as well as sharp gradients into the underlying optimization problems, and it presents new challenges for

*This research is based upon work supported by the United States Air Force Research Laboratory under Contract No. F33615-01-C-3149. Any opinions, findings, conclusions or recommendations expressed in this material are those of the authors and do not necessarily reflect the views of the United States Air Force.

†ALPHATECH, Inc. 6 New England Executive Park, Burlington, MA 01801 kmisovec@alphatech.com

‡Control and Dynamical Systems, California Institute of Technology, Pasadena, CA tinanc@cds.caltech.edu

§ALPHATECH, Inc. 6 New England Executive Park, Burlington, MA 01801 jwohletz@alphatech.com

¶Control and Dynamical Systems, California Institute of Technology, Pasadena, CA murray@cds.caltech.edu

trajectory generation techniques. In this paper, we investigate the use of the nonlinear trajectory generation (NTG) method as a solution to the low-observability path planning challenge.

Trajectory generation algorithms are starting to address the low-observability detectability problem. Work by McFarland et al. [6] uses motion planning techniques using potential field theory for UAV path planning in the presence of detection systems. This is a technique originally used in robot motion planning.

For the low-observability problem, the use of NTG is motivated by recent extensions in its ability to deal with temporal constraints. In [7], NTG is used for a missile intercept problem. In [4], NTG is extended to a multi-vehicle problem with precedence constraints such as *look after strike* and *simultaneous strike*. The low-observability routing problem could be considered to be temporal in nature, by allowing periods of high observability interspersed with periods of low observability. This is desirable because of the way the opponent systems work. Although it might not be possible to get close to the opponent territories while maintaining low-observability at all times; by strategically flying low-observable paths for part of the time, it may be possible to drive the opponent systems into a condition called *lock-loss*. This condition aborts the opponent plans after a specified time of no detection.

Computational efficiency as well as the capability to enforce more realistic constraints, are two additional motivations that have prompted the choice for NTG in past problems. The method combines three technologies- differential flatness, splines and nonlinear optimization and has been extensively investigated [8, 9, 3]. Differentially flat systems have the property that the input variables and states can be written in terms of the output variables and their derivatives. This can aid in computationally efficiency by eliminating the need to integrate as in shooting methods [1]. The use of splines also addresses computational issues by allowing complicated functions to be written with low order polynomials that are active over distinctive intervals.The NPSOL [10] package, which uses sequential quadratic programming, is used in this work as a nonlinear optimization tool.

The contribution of this paper is the application of nonlinear trajectory generation (NTG) methods to generate low-observability routes air vehicles. The aircraft model and detection models are described in the second section. The third section presents an NTG approach formulated for low observability. The fourth section contains examples. The examples demonstrate the ability of NTG to converge to solutions which constrain observability to acceptable levels; however, they also highlight some difficulties with the approach.

2 Model

This section presents the model. These models are based on the Open Experimental Platform (OEP) model developed by Boeing as part of the DARPA MICA program by [2]. In this program, as the problems become progressively more challenging, the models become more refined to capture more realistic features. For the purposes of this report, the models used here are simplified.

The two main components are the aircraft and the detection models, as shown in figure 1. First we discuss the aircraft models, and then the detection models. Throughout this report, we assume that the aircraft maintains a fixed altitude and the radar is on the ground, although the OEP model allows for more complexity. The inputs to the aircraft model include the current aircraft state information, with current waypoint position and velocity, and the destination waypoint position. A constant speed for travel between waypoints is also an input. Note that time could be used as an alternative input to speed, but in the development presented here, we focus on speed. The output of the aircraft model is the aircraft position and attitude in inertial coordinates $(North, East, Up)$.

Figure 2 illustrates an aircraft traveling between waypoints. Important things to note about the point mass model are that changes in speed and heading occur instantaneously at the waypoints, while simple differential equations are used between the waypoints. The equations below represent the state equations for the vehicle traveling from waypoint i to the next waypoint $i+1$.

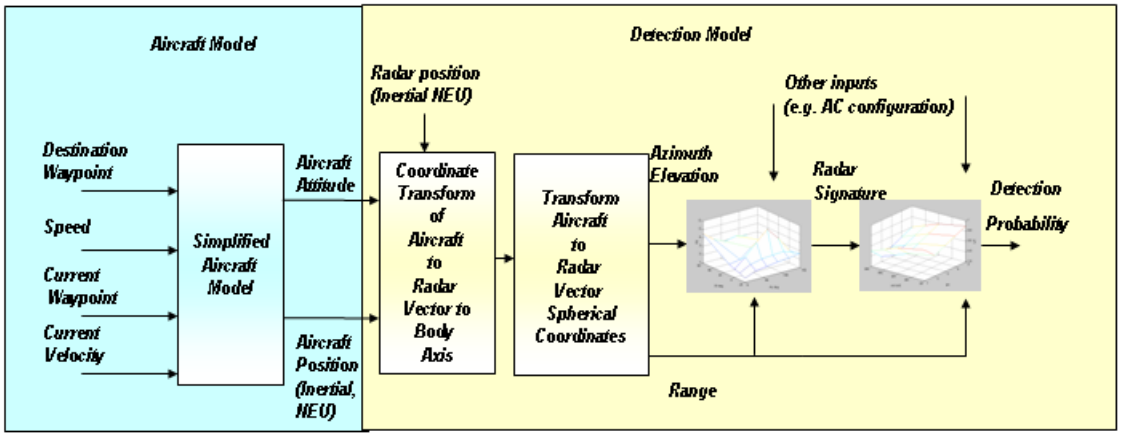

Figure 1: The aircraft dynamics and the detection model comprise two main components of the model.

$$\begin{aligned} \dot{n}_{ac} &= U_i cos(\psi_i) \\ \dot{e}_{ac} &= U_i sin(\psi_i) \\ \dot{h}_{ac} &= 0 \end{aligned} \tag{1}$$

where n_{ac}, e_{ac}, and h_{ac} are the aircraft positions along the north, east and up axes, respectively. U_i is the speed and ψ_i is the heading, which is the angle between the nose and north and is positive clockwise about the *up* axis. Equivalently, assuming that the velocity vector is aligned with the nose, it is useful to write the heading ψ_i as a function of the velocities as follows

$$\psi_i = tan^{-1} \frac{\dot{e}_{ac}}{\dot{n}_{ac}} \tag{2}$$

The aircraft position (n_{ac}, e_{ac}, u_{ac}) is combined with the radar position (n_R, e_R, u_R) to form a vector from the aircraft to the radar.

$$R = (n_R - n_{ac})\hat{n} + (e_R - e_{ac})\hat{e} + (u_R - u_{ac})\hat{u} \tag{3}$$

This vector is then transformed to body axes. Assuming zero pitch and bank angles, for this model, the transformation is

$$R_{body} = \begin{bmatrix} x_{Rac} \\ y_{Rac} \\ z_{Rac} \end{bmatrix} = \begin{bmatrix} cos(\psi) & sin(\psi) & 0 \\ -sin(\psi) & cos(\psi) & 0 \\ 0 & 0 & 1 \end{bmatrix} \begin{bmatrix} (n_R - n_{ac}) \\ (e_R - e_{ac}) \\ (u_R - u_{ac}) \end{bmatrix} \tag{4}$$

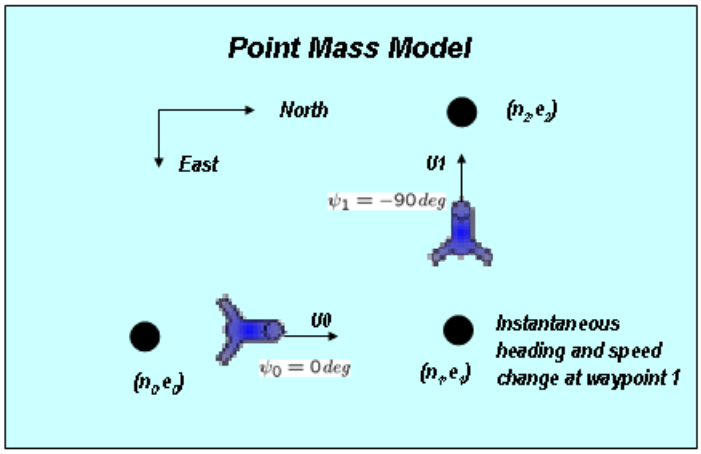

Figure 2: The first version of aircraft model is a point mass model. Speed and heading changes occur instantaneously at the waypoints

The inputs to the detection model are the azimuth, elevation and slant range (az, el, R_s). To obtain these values the vector R_{body} is transformed to spherical coordinates as follows

$$az = tan^{-1}\left(\frac{y_{Rac}}{x_{Rac}}\right) \tag{5}$$

$$el = tan^{-1}\left(\frac{z_{Rac}}{R_g}\right) \tag{6}$$

$$R_s = \sqrt{x_{Rac}^2 + y_{Rac}^2 + z_{Rac}^2} \tag{7}$$

where $R_g = \sqrt{x_{Rac}^2 + y_{Rac}^2}$ is the ground range. Note that since heading is a function of velocities as in equation 2, then these equations can be rewritten as functions of the positions and velocities.

For the next part of the detection model, two tables are used. The tables depend on the type of aircraft, the configuration of the aircraft, as well as the type of radar. In the presentation that follows, we use tables are based on the small UAV with normal configuration and Long Surface Air Missile (SAM) radar model parameters as an example. The first table computes the radar signature given the azimuth and elevation in degrees. The signature is a unitless, intermediary variable that is related to radar cross section. Note for azimuths within +/- 30 degrees ("nose-in" flight), the signature values are lower than for azimuths outside this range ("nose-out" flight). The second table relates the probability of detection with the signature and the slant range.

el /az	0.0	+/-30	+/-31	+/-180
0.0	1.5	1.5	5.5	5.5
+/-20	2.5	2.5	5.5	5.5
+/-45	3.5	3.5	6.0	6.0
+/-90	6.5	6.5	6.5	6.5

Table 1: Signature Values with Respect to Azimuth and Elevation

Signature	Pd=.99	Pd=.5	Pd=.1	Pd=.01
7	380.1	481.2	555.6	656.6
6	213.7	270.6	312.5	369.2
5	120.2	152.2	175.7	207.6
4	67.6	85.6	98.8	116.8
3	38.0	48.1	55.6	65.7
2	21.4	27.1	31.2	36.9
1	12.0	15.2	17.6	20.8

Table 2: Probability of Detection (Pd) Values Respect to Range and Signature

At fixed altitude, it is interesting to consider the how the probability of detection varies with ground range as in figure (3). The figure shows that "nose in" flight is significantly less detectable than "nose out flight". Near 50 km, the approximate range of a homing missile, the detection probabilities vary approximatlely from 0.4 to 0.65. Outside the 80 km radar range, the detection probabilities are zero.

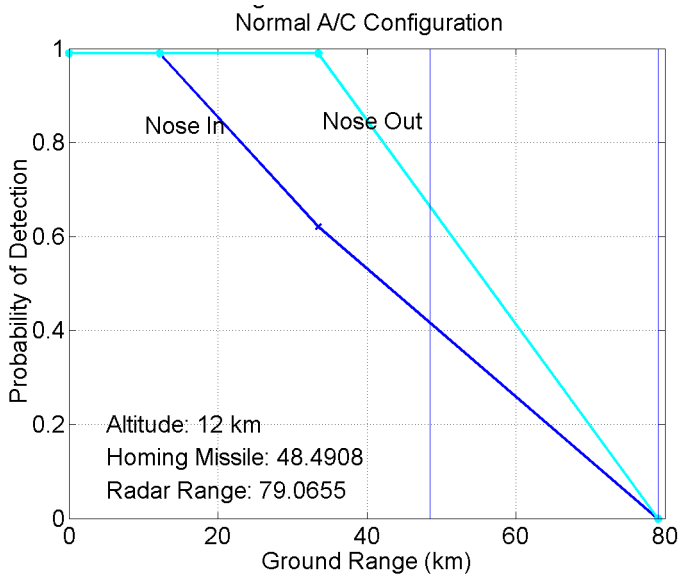

Figure 3: At fixed altitude the probability of detection is smaller for "nose in" flight with azimuths within 30 deg and decreases with increasing ground range

To aid in understanding how the probability of detection varies along various trajectories, we focus on an example where the radar is located at the origin of an inertial coordinate frame with coordinates. An aircraft starts at position (-100 km, -100 km, 12 km) (north, east, up) and may travel along different flight paths. Two flight paths are shown in figure 4. Positions are shown in the (north, east) plane. Times are not indicated on the plot. The trajectory marked with circles is a straight line approach to the origin. The heading is initially 45 degrees, and the azimuth is always near zero. As an airplane following the "circle" trajectory flies closer to the origin, the elevation angle has a larger magnitude and the probability of detection rises. The "plus" trajectory consists of several segments with portions in easterly, northerly and straight line approaches towards the

radar. Note that the occasional sharp changes in the "plus" trajectory occur because the azimuth changes in and out of the +/- 30 degree bound. In the first table, azimuths outside this range yielded higher signatures and consequently higher probability of detections.

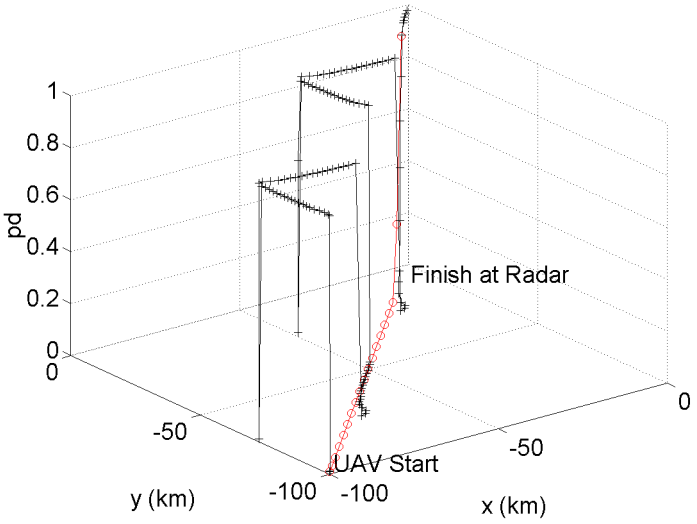

Figure 4: Probability of Detection exhibits sharp gradients and path dependencies.

From the two tables, an analytical observability model, generically shown in equation (8) can be developed using any number of function approximation techniques.

$$sig = sig(az, el)$$
$$p_d = p_d(R, sig)$$

We have used the B–spline curve fits because of their flexibility and ease of computing their derivatives to find an analytical model for the signature data given in table 1. Figure (5) shows the result of the fit function model of the signature values by B–spline tensor product functions versus the actual data points indicated by 'o'. The probability of detection table can be fit in a similar fashion.

Then the problem is to find trajectories for the dynamic system in equation (1) such that the trajectories are optimized with respect to the detection models described in this section. This section illustrates that even for highly simplified models, the optimization of trajectories for low observability flight can be quite challenging.

3 Approach

In this section, we first briefly outline the NTG algorithm with temporal constraints and then describe our approach to the low observability trajectory optimization problem formulation. Illustrative examples will be given in the next section.

3.1 Brief Summary of NTG Algorithm

The baseline NTG algorithm has been described extensively in the literature [7, 9, 8, 3], therefore in this section we outline it briefly.

The NTG software package is based on a combination of nonlinear control theory, spline theory and sequential quadratic programming. There are three steps in NTG algorithm. The first step is to use the differential flatness property to find a new set of outputs of a system so that the

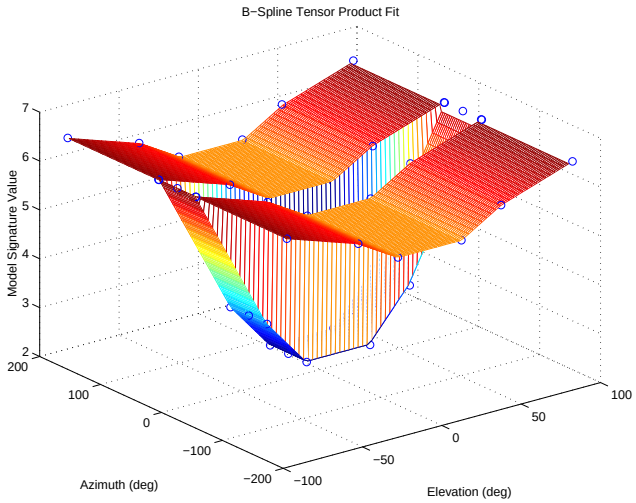

Figure 5: The Signature Data Fit Function by B–Spline Tensor Product Functions.

system dynamics can be mapped down to a lower dimensional space. All the states and controls of the system must be recovered from the new lower dimensional representation of the system. Let's consider a nonlinear system given by:

$$\dot{x} = f(x, u) \tag{8}$$

where $x \in R^n$ and $u \in R^m$ represents the states and the inputs, respectively. It is assumed that all vector fields and functions are real–analytic. The goal is to find a minimizing trajectory of the system given in equation (8) for the following cost function (J) which consists of initial (ϕ_0), final (ϕ_f) and trajectory (L) cost functions;

$$J(x, u) = \phi_0(x(t_0), u(t_0)) + \phi_f(x(t_f), u(t_f)) + \int_{t_0}^{t_f} L(x(t), u(t))dt \tag{9}$$

The system given in equation (8) is subject to the following constraints;

$$\begin{aligned} lb_0 \leq \psi_0(x(t_0), u(t_0)) \leq ub_0 \qquad & N_0 \text{ initial constraints} \\ lb_f \leq \psi_f(x(t_f), u(t_f)) \leq ub_f \qquad & N_f \text{ final constraints} \\ lb_t \leq \psi_t(x(t), u(t)) \leq ub_t \qquad & N_t \text{ trajectory constraints} \end{aligned} \tag{10}$$

The system in equation (8) can be mapped to a lower dimensional space, in which it will be easier and computationally more efficient to solve the optimization problem, by finding an output $z = z_1, \cdots, z_q$ of the form

$$z = A\left(x, u, u^{(1)}, \cdots, u^{(r)}\right) \tag{11}$$

where $u^{(i)}$ denotes ith derivative of u respect to time.

If equation (8) is differentially flat then the states and inputs of the system, (x, u), can be completely established from equation (12). If there is no flat output exists or one cannot find a flat output, then (x, u) can still be completely determined from the lowest dimensional space possible given in equation (13). A necessary condition for the existance of such outputs is given in [5].

$$(x, u) = B\left(z, z^{(1)}, \cdots, z^{(s)}\right) \tag{12}$$

$$\begin{aligned}(x, u) &= B_1\left(z, z^{(1)}, \cdots, z^{(s_1)}\right) \\ (x, u) &= B_2\left(z, z^{(1)}, \cdots, z^{(s_2)}\right)\end{aligned} \tag{13}$$

where $z^{(i)}$ denotes ith derivative of z respect to time.

The second step in NTG is to further represent these outputs in terms of the B–spline functions as

$$z_j(t) = \sum_{i=1}^{p_j} B_{i,k_j}(t) C_i^j \qquad \text{for the knot sequence} \quad t_j, \;\; j = 1, \cdots, q$$

where $B_{i,k_j}(t)$ represents the B–spline basis function for the output z_j with the degree of spline polynomial k_j. C_i^j represents the coefficients of the B–splines, l_j is the number of knot intervals, and m_j is the number of smoothness conditions at the knot points, p_j is the number of coefficients of the each output given by

$$p_j = l_j(k_j - m_j) + m_j$$

Finally to solve the coefficients of the B–spline functions by sequential quadratic programming package NPSOL, the cost function and constraints given in equations (9) and (10), respectively, are re–formulated in terms of the B–spline coefficients. Therefore, the problem now can be stated as the following nonlinear programming form:

$$\min_{y \in R^M} \;\; F(y) \qquad \text{subject to} \qquad lb \leq c(y) \leq ub$$

where $J(x, u) \rightarrow F(y)$ and $\{\phi_0(x(t_0), u(t_0)), \;\; \phi_f(x(t_f), u(t_f)), \;\; \phi_t(x(t), u(t))\} \rightarrow c(y)$

$y = \left(C_1^1, \cdots, C_{p_1}^1, \cdots, C_1^q, \cdots, C_{p_q}^q\right)$ and $M = \sum_{i=1}^{q} p_i$

3.2 Using Temporal Constraints with NTG

While the NTG formulation allows any spatial constraint to be easily coded into the constraint set, including temporal constraints requires more care. [7, 4]. A key idea in the temporal formulation of NTG is to let event times become state variables in the optimization. This allows precedence constraints to be included in the optimization by equations relating the event times. For example suppose that n events occur at T_i for $i = 0, 1, \cdots, n-1$. In equation (14), we define τ as a scaled time variable. It is equal zero when time, t, is equal to zero, but it is equal to one when all events have occurred at $T = \sum_{i=0}^{n-1} T_i$. In the setup of the optimization problem, which will be detailed below, scaled time τ rather than time t is used. In the optimization details below, the use of new time variable, τ, has implications for the way integrals and derivatives are written. For example, derivatives with respect to t become derivatives with respect to τ with the chain rule as in equation (15).

$$\tau = \frac{t}{T} \tag{14}$$

$$\frac{d}{dt} \rightarrow \frac{d}{d\tau}\frac{d\tau}{dt} = \frac{1}{T}\frac{d}{d\tau} \tag{15}$$

As a result, after introducing new state variable T, cost and constraint functions given in equations (9) and (10) become

$$J(x, u, T) = \phi_0(x(0), u(0), T) + \phi_f(x(1), u(1), T) + \int_0^1 L(x(\tau), u(\tau), T)d\tau \tag{16}$$

$$\begin{aligned} lb_0 \leq \psi_0(x(0), u(0), T) \leq ub_0 \qquad & N_0 \text{ initial constraints} \\ lb_f \leq \psi_f(x(1), u(1), T) \leq ub_f \qquad & N_f \text{ final constraints} \\ lb_t \leq \psi_t(x(\tau), u(\tau), T) \leq ub_t \qquad & N_t \text{ trajectory constraints} \end{aligned} \tag{17}$$

There will be also additional temporal constraints which can be expressed as a set of inequalities given below

$$lb_T \leq \psi_T(T) \leq ub_T \qquad N_T \text{ temporal constraints}$$

3.3 Formulation of the Low Observability Problem

Now that we have outlined the general methods, we focus on how to apply these methods to the low observability problem. Define a set of event times T_{2i} and T_{2i+1} for $i = 0, 1, \cdots, n$ and the number of events $2n + 1$ is specified. We will set up events such that periods of low observability $T_{2i-1} \leq t \leq T_{2i}$ are interspersed with times of high observability, $T_{2i} \leq t \leq T_{2i+1}$.

The system dynamics for this problem consist of the vehicle dynamics in equation (1) together with the following dynamics on the new state variables

$$\frac{dT_{2i}}{d\tau} = 0$$

$$\frac{dT_{2i+1}}{d\tau} = 0 \qquad i = 0, ...n$$

Note that the system is differentially flat. All variables of interest can be written as a function of the output variables, x, y, T_{2i}, T_{2i+1} and their derivatives, where x and y denote north and east positions respectively of an aircraft. The observability model in equation (8) is a function of the flat variables, and is used in the optimization below.

Next, we develop a set of cost and constraint functions. Note that we will develop a general set, with design options to eliminate some components of the cost and constraint functions. A cost function, J, is shown in equation (18). The first term in the cost function is standard in the temporal approach. Since T is the mission time as shown in equation (19), this term acts to minimize the total mission time. The second term is a speed penalty. It has also been used in the past as a way to penalize control action. The third and fourth terms are cumulative penalities on observability. Since probability of detection and signature are always non-negative, these terms are appropriate and may be useful. W_u, W_p and W_s represent the weight functions on the speed, probability and signature penalties, respectively. The integral in equation (18) is respect to the scaled time, τ, and has bounds from zero to one. The cost function presented here is a classic tradeoff between various performance measures and control action measures.

$$J = T^2 + \int_0^1 \left(W_u \frac{1}{T^2} \left(\left(\frac{dx}{d\tau} \right)^2 + \left(\frac{dy}{d\tau} \right)^2 \right) + W_p p_d + W_s sig \right) T d\tau \tag{18}$$

where

$$T = \sum_{i=0}^{n-1} (T_{2i} + T_{2i+1}) \tag{19}$$

Next we present a set of constraints, and we divide the constraints into subsets based on the type of constraint used. First there are constraints on the initial conditions for the variables. There are linear constraints as in equation (20) on the initial position and event times. The initial condition constraints on velocities become nonlinear because of the differentiation with respect to scaled time shown above in equation (15). The constraints on velocities are presented in equation (21).

$$\begin{aligned} x(0) \leq x(\tau)|_{\tau=0} \leq x(0) \\ y(0) \leq y(\tau)|_{\tau=0} \leq y(0) \\ minT_{2i} \leq T_{2i}|_{\tau=0} \leq maxT_{2i} \\ minT_{2i+1} \leq T_{2i+1}|_{\tau=0} \leq maxT_{2i+1} \end{aligned} \tag{20}$$

$$\begin{aligned} T\dot{x}(0) \leq \frac{dx}{d\tau}|_{\tau=0} \leq T\dot{x}(0) \\ T\dot{y}(0) \leq \frac{dy}{d\tau}|_{\tau=0} \leq T\dot{y}(0) \end{aligned} \tag{21}$$

where $\dot{(\cdot)} = \frac{d(\cdot)}{dt}$

Speed and radius of curvature limits are nonlinear functions of scaled time. Constraints for these are shown in equations (22) and (23). Note that the equations are scaled to aid in convergence of the nonlinear optimization codes.

$$\frac{v_{min}^2}{v_{max}^2} \leq \frac{1}{T^2} \left(\left(\frac{dx}{d\tau} \right)^2 + \left(\frac{dy}{d\tau} \right)^2 \right) \leq 1 \tag{22}$$

$$\frac{\rho_{min}}{\rho_{max}} \leq \frac{\frac{dx}{d\tau}\frac{d^2y}{d\tau^2} - \frac{dy}{d\tau}\frac{d^2x}{d\tau^2}}{\left(\left(\frac{dx}{d\tau} \right)^2 + \left(\frac{dy}{d\tau} \right)^2 \right)^{1.5}} \leq 1 \tag{23}$$

Finally, constraints on observability can be included. Consider a constraint on signature as in equations (24). In order to circumvent difficulties with discontinuous constraints, which are

not permitted with the NTG method, a single constraint on signature is represented with two continuous constraints. During the different low or high observability events, only one of these two constraints is active. During low-observable times the signature is constrained to be low as in the first equation in the set of equations in (24). The second constraint in the second line of (24) is present, but is automatically satisfied if the first constraint is satisfied. During the times of high-observability, the fourth equation in (24) allows the signature to reach its high value. The constraint in the third line of (24) is present, but is automatically satisfied.

$$\begin{aligned} T_{2i} \le t \le T_{2i+1} \qquad & 0 \le sig \le sig_L \\ & 0 \le sig \le sig_H \\ T_{2i+1} \le t \le T_{2i+2} \qquad & 0 \le sig(T_{2i}) \le sig_L \\ & 0 \le sig \le sig_H \end{aligned} \tag{24}$$

Constraints on probability of detection can be included in a similar fashion shown in equation (25).

$$\begin{aligned} T_{2i} \le t \le T_{2i+1} \qquad & 0 \le p_d \le p_{d_L} \\ & 0 \le p_d \le p_{d_H} \\ T_{2i+1} \le t \le T_{2i+2} \qquad & 0 \le p_d(T_{2i}) \le p_{d_L} \\ & 0 \le p_d \le p_{d_H} \end{aligned} \tag{25}$$

Note that the constraints on signature and probability of detection are nonlinear function of scaled time and are represented in the NTG code similarly to speed and curvature limits.

The last constraint in equation (26) ensures that the vehicle reaches the destination waypoint, (x_{dw}, y_{dw}), within a radius bound e_{min} and e_{max}. This constraint is nonlinear, and it is a function of the final scaled time, $\tau = 1$, which corresponds to unknown actual final time of t_f.

$$\frac{e_{min}^2}{e_{max}^2} \le (x(1) - x_{dw}(1))^2 + (y(1) - y_{dw}(1))^2 \le 1 \tag{26}$$

4 Examples

In this secton, illustrative examples to our approach for the real time low observability nonlinear trajectory generation problem are given. We assume that altitude is fixed at 12 km. The initial location of the aircraft is at (-100 km, -100 km), and there is a radar located at the origin. Note that the difficulties with flying trajectories in these examples were highlighted earlier in figure (4). In the examples below, the aircraft travels to a target located at (5 km, -15 km). The examples highlight the ability of the temporal methods to design for distinct periods of high and low observability. However, they also demonstrate sensitivity to the initial coarse route.

Figure (6) results from a simulation in which the initial coarse route input to the NTG algorithm is at (-100km, -15 km). Figure (6)(a) shows that the optimized path first circles through the left side of the radar, thereby constraining the signature value of the aircraft during the low-observability event as shown in figure (6)(b). In this example the low signature bound is at 4.2. After a period of constrained low signature, the signature is allowed to increase to the maximum value at 6.5.
If NTG is initially fed with a better course route (0, -100 km), then NTG produces a different solution as illustrated in figure (7). In this example the UAV flies "nose in", with low azimuths, directly toward the target. The signature values are lower than in the first example. Figure (8) is included to highlight the distinct periods of high or low signatures.

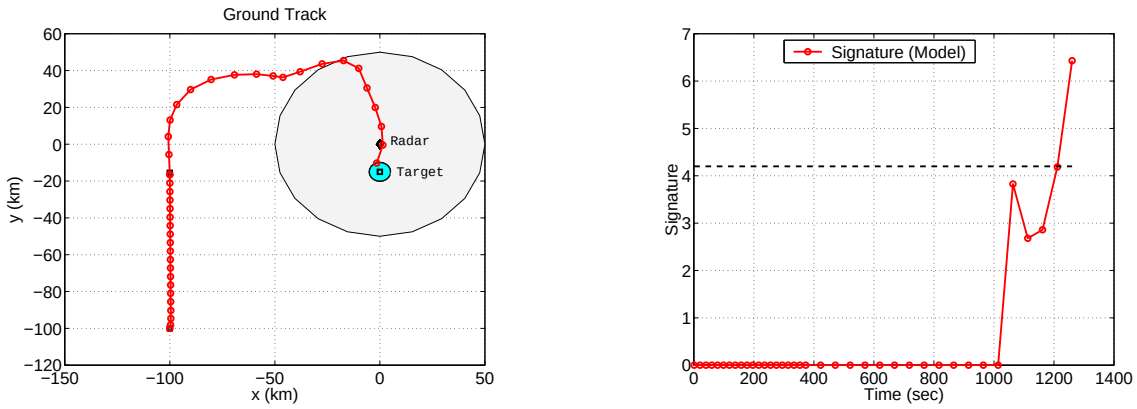

(a) (b)

Figure 6: (a) Ground Track of the Optimized Path for Low Observability (b) Signature Value Across the Optimized Path for Low Observability

5 Conclusions

Low observability flight path planning in the presence of RADAR detection systems is a new controls challenge that will increase capabilities for unmanned air vehicles. Simple aircraft models coupled with detection models illustrate complex behavior. Path dependencies and multiple minima are features that make the underlying optimization difficult. Explorations with variations of the nonlinear trajectory generation methods are capable of producing solutions that satisfy observability constraints. The solutions highlight interesting problems for future work such as coupling NTG with a coarse but global optimizer.

References

[1] John T. Betts. *Practical Methods for Optimal Control Using Nonlinear Programming*. Society of Industrial and Applied Mathematics, 2001.

[2] Corman D. and Knutti J. Mica oep 1.1 user guide. *The Boeing Company Internal Report*, 2003.

[3] Lian F.-L. and Murray R.M. Real-time trajectory generation for the cooperative path planning of multi-vehicle systems. *Conference on Decision and Control*, 2002.

[4] Lian F.-L. and Murray R.M. Cooperative task planning of multi-robot systems with temporal constraints. *To appear in International Conference on Robotics and Automation*, 2003.

[5] Fliess M., Levine J., Martin P., and Rouchon P. Flatness and defect of nonlinear systems: Introductory theory and examples. *International Journal of Control (61)6 1327-1360*, 1995.

[6] McFarland M.B. and Acjeru R.A. amd Taylor B.K. Motion planning for reduced observability of autonomous aerial vehicles. *IEEE International Conference on Control Applications*, 1999.

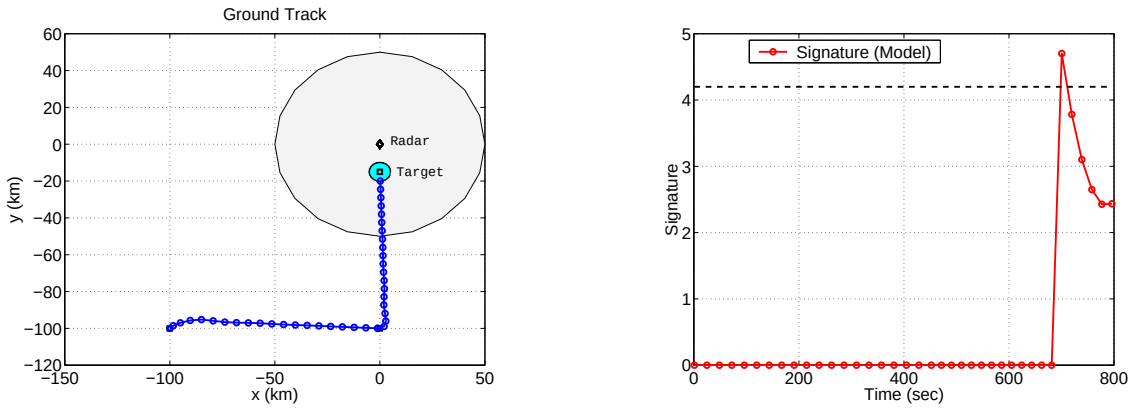

(a) (b)

Figure 7: (a) Ground Track of the Optimized Path for Low Observability with Better Initial Course Route (b) Signature Value Across the Optimized Path for Low Observability with Better Initial Course Route

[7] Milam M.B. Missile interception research report. *California Institute of Technology Internal Report*, 2002.

[8] Milam M.B., Mushambi K., and Murray R.M. A computational approach to real-time trajectory generation for constrained mechanical systems. *Conference on Decision and Control*, 2000.

[9] Milam M.B., Franz R., and Murray R.M. Real-time constrained trajectory generation applied to a flight control experiment. *IFAC*, 2002.

[10] Gill P.E., Murray W., Saunders M.A., and Wright M. H. User's guide for npsol 5.0 a fortran package for nonlinear programming. *Systems Optimization Laboratory, Stanford University, Stanford CA*, 1998.

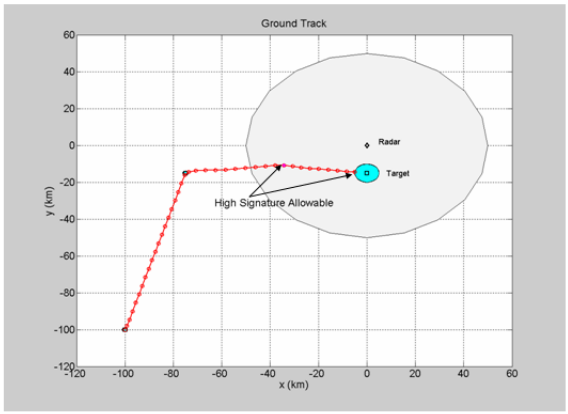

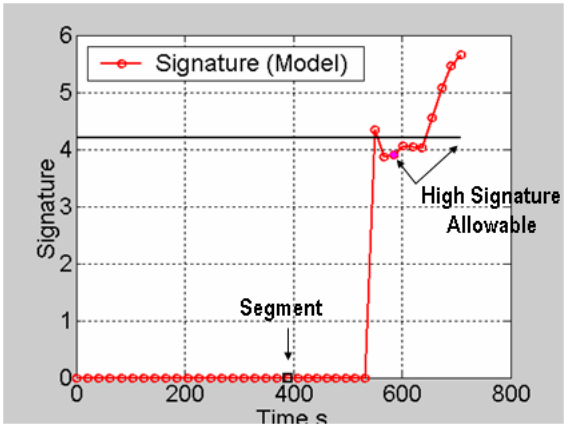

(a) (b)

Figure 8: (a) Ground Track of the Optimized Path for Low Observability (b) Signature Value Across the Optimized Path for Low Observability